HHS Public Access

Author manuscript

IEEE Trans Biomed Eng. Author manuscript; available in PMC 2018 March 01.

Published in final edited form as:

IEEE Trans Biomed Eng. 2017 March ; 64(3): 681–689. doi:10.1109/TBME.2016.2572678.

Intratidal Overdistention and Derecruitment in the Injured Lung: A Simulation Study

Reza Amini,
Beth Israel Deaconess Medical Center and Harvard Medical School, Boston MA, USA. He is with Cimetrics, Inc., Boston, MA, USA

Jacob Herrmann, and
University of Iowa, Iowa City, IA, USA

David W. Kaczka* **[Member, IEEE]**
University of Iowa, Iowa City, IA, USA

Abstract

Goal—Ventilated patients with the Acute Respiratory Distress Syndrome (ARDS) are predisposed to cyclic parenchymal overdistention and derecruitment, which may worsen existing injury. We hypothesized that intratidal variations in global mechanics, as assessed at the airway opening, would reflect such distributed processes.

Methods—We developed a computational lung model for determining local instantaneous pressure distributions and mechanical impedances continuously during a breath. Based on these distributions and previous literature, we simulated the within-breath variability of airway segment dimensions, parenchymal viscoelasticity, and acinar recruitment in an injured canine lung for tidal volumes (V_T) of 10, 15, and 20 mL kg^{-1} and positive end-expiratory pressures (PEEP) of 5, 10, and 15 cm H_2O. Acini were allowed to transition between recruited and derecruited states when exposed to stochastically-determined critical opening and closing pressures, respectively.

Results—For conditions of low V_T and low PEEP, we observed small intratidal variations in global resistance and elastance, with a small number of cyclically recruited acini. However with higher V_T and PEEP, larger variations in resistance and elastance were observed, and the majority of acini remained open throughout the breath. Changes in intratidal resistance, elastance, and impedance followed well-defined parabolic trajectories with tracheal pressure, achieving minima near 12 to 16 cm H_2O.

Conclusion—Intratidal variations in lung mechanics may allow for optimization of ventilator settings in patients with ARDS, by balancing lung recruitment against parenchymal overdistention.

Significance—Titration of airway pressures based on variations in intratidal mechanics may mitigate processes associated with injurious ventilation.

correspondence: david-kaczka@uiowa.edu.

Index Terms

Biological models; computational models; lung pathology; mechanical ventilation; respiratory mechanics

I. Introduction

The Acute Respiratory Distress Syndrome (ARDS) is characterized by airway closure / atelectasis, alveolar flooding, increased lung resistance, and reduced lung compliance. For patients meeting the clinical criteria for ARDS, the mortality rate is about 40%. Supportive mechanical ventilation is the mainstay of the treatment, with one therapeutic goal being improvement in gas exchange. However positive pressure ventilation may worsen lung injury, due to parenchymal overdistention (volutrauma) and repetitive recruitment / derecruitment (atelectrauma). The mechanical stresses associated with these processes result in the release of cytokines and other inflammatory mediators (biotrauma) that may lead to further injury, maldistribution of ventilation, and additional impairments in gas exchange. Therefore treatment goals for 'lung-protective' ventilation are to minimize volutrauma by selection of an appropriate tidal volume (V_T), and to minimize atelectrauma by appropriate positive end-expiratory pressure (PEEP).

In the ventilated patient, optimization of PEEP and V_T often depends on quantitative assessments of airway pressure, as a surrogate indicator of parenchymal stress [1, 2]. Such assessments may include the concavity of the airway pressure vs. time tracing [3, 4], so-called 'best' compliance [5–7], or nonlinear distortions of elastance [8, 9]. More recent studies have adjusted PEEP or V_T based on measurements of esophageal pressure to estimate transpulmonary pressure, rather than transrespiratory pressure [10]. Despite promising preliminary results, it is still unclear whether measures of esophageal pressure will present a clinically useful technique to adjust ventilator settings [11].

We hypothesized that intratidal variations in global lung mechanics, as assessed at the airway opening, would be a sensitive indicator of these pathophysiologic processes. To test this hypothesis, we developed a computational lung model for determining local instantaneous pressure distributions and mechanical impedances continuously during a breath. Our model incorporates specific pathophysiologic processes for acinar recruitment / derecruitment (R/D) and parenchymal overdistention, typical of what has been observed experimentally in canine acute lung injury [12, 13]. The specific objectives of this study were to: 1) develop a computational model of the injured canine lung incorporating parenchymal overdistention, as well as within-breath recruitment and derecruitment; 2) determine how these processes impact local (acinar) and global (whole lung) mechanical behavior for various PEEP and V_T settings; and 3) assess whether intratidal variations in global lung mechanics allow for the optimization of PEEP and V_T.

Portions of this work were presented in abstract form at the 2010 Annual Meeting of the Biomedical Engineering Society in Austin, TX [14].

II. Materials and Methods

A. Model Structure

The structure of the model is based on a 47-order, asymmetric binary airway tree of the canine lung [15], consisting of K = 300,153 discrete airway segments (i.e., nodes), including N = 150,077 terminal bronchioles. Each k^{th} airway segment was assumed to behave as a simple distensible cylinder, with length and diameter varying with the cube root of the local instantaneous transmural pressure [16, 17]. Longitudinal impedance for each airway segment depends on the airway segment dimensions, as well as physical gas properties [18]. Viscoelastic airway wall properties were simulated using the appropriate distributions of cartilage and soft tissue for each order [19]. An additional shunt impedance was included to account for the adiabatic compression of gas contained within each airway segment [17]. Each terminal airway segment was subtended by a viscoelastic "constant-phase" acinus with index n [20]. Each acinus was characterized by a tissue elastance parameter (H_n), as well as a dimensionless tissue hysteresivity parameter (η_n) to account for dynamic pressure-volume hysteresis [21]. To simulate parenchymal overdistention [22], both H_n and η_n were allowed to vary as functions of the local instantaneous transpulmonary pressure ($P_{tp,n}$) over the course of a breath, according to the quadratic relationships [17,22]:

$$H_n\left(P_{tp,n}\right)=1.724-0.0511P_{tp,n}+0.013P_{tp,n}^2 \quad (1)$$

$$\eta_n\left(P_{tp,n}\right)=0.2832-0.0248P_{tp,n}+0.0008P_{tp,n}^2 \quad (2)$$

where $P_{tp,n}$ is expressed in units of cm H_2O, H_n is expressed in units of cm H_2O μL^{-1}, and η_n is dimensionless [21]. Equations (1) and (2) thus allow for empirically nonlinear increases in parenchymal tissue elastance and resistance (as determined from the product of H_n and η_n) with distending pressure [22].

The R/D processes were determined according to stochastically assigned values for critical opening / closing pressures for each acinus ($P_{crit,n}$). To determine the distribution of these critical pressures, we reanalyzed the previously published data of Kaczka et al. [13], who reported global dynamic elastance in canines before and after oleic acid-induced lung injury. We found that the ratio of their measured baseline elastance to injured elastance, which is reflective of lung recruitment [23], followed a linear relationship with distending pressure from 5 to 20 cm H_2O (Fig. 1-a). We therefore assumed that the slope of the regressed line describing this relationship between the percentage of recruited lung and distending pressure was equivalent to the cumulative distribution of acinar values for $P_{crit,n}$ in the model (Fig. 1-b). Using this linear regression, our model assumed that approximately 7.6% of the lung is recruited at a distending pressure of 0 cm H_2O, and that 100% of the lung is recruited at about 28 cm H_2O. We also constrained acinar recruitment to occur only during inhalation, while derecruitment occurred only during exhalation.

B. Simulations

A numerical algorithm was used to simulate local, instantaneous time-domain variations in regional flow and pressure throughout the airway tree during sinusoidal excitation (Fig. 2). Nonlinear alterations in regional impedance were assumed to arise from intratidal variations in airway size, parenchymal strain-stiffening, and acinar R/D. The algorithm was initiated at time $t = 0$ seconds, by setting a specified PEEP, V_T, and frequency (f, expressed in units of Hz). The trachea of the model was assumed to be driven by an input sinusoidal flow ($\dot{V}_{tr}$) with amplitude:

$$\left|\dot{V}_{tr}\right| = \pi f V_T \quad (3)$$

The percentage of derecruited acini for the starting condition of the model was determined according to the linear regression of Fig. 1-a. A derecuited acinus was assumed to have an impedance value of $10^{16} + j10^{16}$cm H_2O s μL^{-1}, which is several orders of magnitude higher than the wall or gas compression impedances of its corresponding terminal bronchiole [18]. When an acinus transitioned from a derecruited state to a recruited state, we assumed that it instantly inflated to its appropriate volume for the corresponding distending pressure, $P_{crit,n}$. In other words, its pressure-volume characteristic was preserved [24].

The mechanical impedance looking into each node of the tree (Z_k) was determined in the frequency-domain at this instant of time from the complex summation of all airway, gas compressive, and parenchymal tissue impedances in the appropriate serial and parallel fashion [18]. Global lung impedance (Z_L) was defined as the total mechanical impedance to flow at the trachea. Local flow ($\dot{V}_k$) and pressure (P_k) distributions throughout the tree were determined using a recursive flow-divider algorithm with preorder traversal sequence [25]. All impedance values, flows, and pressures within the tree were complex values with both real and imaginary components, or equivalently, magnitudes and phases. At each airway node k, the local pressure magnitudes ($|P_k|$) and phases (ϕ_k) at the discrete frequency f were converted to an equivalent time-domain value at time t according to:

$$P_k(t) = |P_k| \cos(2\pi f t + \phi_k) \quad (4)$$

The time index was then incremented as $t = t + dt$, and each $P_k(t)$ in the model was updated. All local impedances and acinar R/D states were recalculated at the new local distending pressures, according to (4). This process was repeated until $t = t_{max}$, when the simulation was terminated.

All simulations were performed assuming a 25 kg dog with functional residual capacity of about 1.3 liter at 5 cm H_2O distending pressure. In practice, we simulated three complete breaths with a respiratory rate of 20 min^{-1} ($f = 0.333$ Hz) at 25 points per breath ($dt = 0.125$ s), PEEPs of 5, 10, and 15 cm H_2O, and V_T of 10, 15, and 20 mL kg^{-1}. However we restricted our analysis only to the third breath, to minimize the influence of any numerical transient responses. Total lung impedance Z_L as measured at the trachea was determined at

each instant of time throughout the course of a breath, along with global lung resistance and elastance as R_L = Re{Z_L} and E_L = -2πfIm{Z_L}, respectively. The tracheal pressure (P_{tr}) at a specific instant of time was first computed in the frequency-domain as

$$P_{tr}(f)=Z_L(f)\dot{V}_{tr}(f) \quad (5)$$

which was converted to its time-domain equivalent according to (4). Given that the nonlinear processes of intratidal overdistention and R/D occurred over the course of a breath, we then estimated the degree of nonlinear distortion in P_{tr} using the harmonic index κ_d of Zhang et al. [26]:

$$\kappa_d=\sqrt{\frac{\mathscr{P}_{ni}}{\mathscr{P}_{tot}}}\times 100\% \quad (6)$$

where $\mathscr{P}_{tot}$ is the total spectral power in P_{tr}, and $\mathscr{P}_{ni}$ is the power in P_{tr} only at those frequencies in the input $\dot{V}_{tr}$ signal with no spectral energy. Thus if the P_{tr} waveform corresponded to a pure sinusoid, then κ_d = 0. In addition, we performed multiple linear regression on the tracheal pressure, flow, and volume data from the single breath in the time-domain [27] using the following equation of motion:

$$P_{tr}(t)=R\dot{V}_{tr}(t)+E_1V_{tr}(t)+E_2V_{tr}^2(t)+E_3V_{tr}^3(t)+\mathrm{PEEP} \quad (7)$$

where R denotes an estimated linear coefficient of lung resistance, E_1, E_2, and E_3 are polynomial coefficients of lung elastance, and V_{tr} denotes delivered volume at the trachea at time t. Equation (7) assumes that the relationship between tracheal pressure and volume is best characterized by a cubic polynomial [28]. Based on estimates of these elastance coefficients, we determined an extended version of a nonlinear volume-dependent elastance index [4, 9, 29]:

$$\%E_3=\frac{E_2V_T+E_3V_T^2}{E_1+E_2V_T+E_3V_T^2}\times 100\% \quad (8)$$

where $\%E_3$ denotes the percentage of nonlinear elastic recoil.

For the purpose of assessing the local mechanics of the injured lung, we characterized the acinar flow patterns into three distinct subgroups as illustrated in Fig. 3: (a) those that were consistently recruited and received advective flow during the course of the entire breath; (b) those that were transitional and were either recruited and / or derecuited during the breath; and (c) those that were consistently derecruited and received no flow at any time point in the breathing cycle. Thus consistently recruited acini have the highest potential for overdistension, consistently-derecruited do not participate in gas exchange, and transitional

acini are at the highest risk for atelectrauma. In addition, we defined a so-called 'recruitment duty cycle' for each acinus (RDC_n) as the amount of time that the acinus remains in the recruited state ($T_{rec,n}$) divided by the total duration of the breath (T_{tot}):

$$\mathrm{RDC}_n = \frac{T_{rec,n}}{T_{tot}} \quad (9)$$

Thus the RDC_n for consistently recruited acini would be 1, consistent derecuited acini would be 0, and transitional acini would be between 0 and 1. RDC_n histograms for each PEEP and V_T were constructed with bin sizes of 0.08333. Finally we examined total lung dynamic pressure-volume (P-V) loops for the individual breaths at each PEEP and V_T, by plotting tidal volume against the absolute P_{tr} during inspiration and expiration.

All algorithms were written and executed using Matlab v7.0 (The Mathworks, Natick, MA). Total computation time for one simulation at a specified V_T and PEEP was approximately 12 hours using a Dell desktop computer with an Intel Pentium® 4 processor running Windows 32 bit operating system at 2.80 GHz and 3.42 GB RAM.

III. Results

Fig. 4 shows the percentages of consistently recruited, transitional, and consistently derecruited acini in the model for 5, 10, and 15 cm H_2O PEEP and 10, 15, and 20 mL kg^{-1} V_T. For our simulated conditions, the greatest percentage of consistently derecruited acini was about 38%, which occurred at the lowest PEEP of 5 cm H_2O, and lowest V_T of 10 mL kg^{-1}. The amount of derecruited acini at this PEEP decreased to about 16% for 15 mL kg^{-1} V_T. The percentage of consistently recruited acini remained constant with V_T for each PEEP level, but increased as PEEP increased. The relative number of transitional acini increased with increasing V_T for 5 cm H_2O PEEP, from about 38% at V_T = 10 mL kg^{-1} to about 76% at V_T = 20 mL kg^{-1}. Consistently derecruited acini occurred only at V_T of 10 and 15 mL kg^{-1} for 5 cm H_2O PEEP, and only at V_T of 10 mL kg^{-1} for 10 cm H_2O PEEP. For 5 and 10 cm H_2O PEEP, transitional acini increased with increasing V_T. However for a given PEEP, the number of consistently recruited acini remained unchanged with V_T. Fig. 5 shows the distribution of acinar recruitment duty cycles (RDC_n). Consistent with Fig. 4, these histograms demonstrate that for a given PEEP, the number of transitional acini at a specified RDC value generally increased with increasing V_T. However, the time that transitional acini remained in a recruited state (i.e., $T_{rec,n}$), increased with both PEEP and V_T.

Fig. 6 shows the within-breath variations of P_{tr}, R_L, E_L, $|Z_L|$, as well as the percentage of recruited acini as functions of time. The peak P_{tr} increased with both PEEP and V_T. The smallest peak P_{tr} occurred at PEEP of 5 cm H_2O and V_T of 10 mL kg^{-1}, while the largest occurred at PEEP of 15 cm H_2O and V_T of 20 mL kg^{-1}. The greatest variations in R_L, E_L, and $|Z_L|$ occurred for V_T of 20 mL kg^{-1}, regardless of PEEP. Within-breath variations in these three parameters closely followed the corresponding temporal variations in P_{tr}. However for 5 and 10 cm H_2O PEEP, the R_L, E_L, and $|Z_L|$ exhibited slight decreases at the

beginning of the breath and slight increases at the end of the breath. The degree of harmonic distortion in P_{tr}, κ_d, also increased with both PEEP and V_T, with values ranging between 7.53% to 35.4% (Table I). The $\%E_3$ index demonstrated more complicated behavior (Table II). At PEEP of 5 cm H_2O, $\%E_3$ yielded negative values for all V_T, although its magnitude decreased with increasing V_T. However at PEEP of 10 and 15 cm H_2O, $\%E_3$ was positive for all V_T, and generally increased with increasing V_T. The smallest magnitude of $\%E_3$ (7.3%) occurred at PEEP of 10 cm H_2O and V_T of 10 mL kg^{-1}. Regardless of PEEP or V_T, the R_L, E_L, and $|Z_L|$ followed well-defined, parabolic trajectories with P_{tr}, achieving minima at 15.9, 11.6, and 11.6 cm H_2O, respectively (Fig. 7).

Fig. 8 shows the dynamic P-V loops for individual breaths at each PEEP and V_T. The loops are color-coded to indicate the percentage of recruited lung during the inspiratory and expiratory portions of the breath. For each V_T, the P-V loops were shifted toward the right with increasing PEEP. Lung volume exhibited a near-linear relationship with P_{tr} for pressures less than 25 cm H_2O. Characteristic flattening of the loops near end-inspiration occurred above 28 cm H_2O, and only when the lung was 100% recruited.

IV. Discussion

In this study, we developed a computational lung model to simulate within-breath variations in airway segment dimensions, parenchymal viscoelasticity, and acinar R/D in an injured canine lung during physiological PEEP and V_T. Our model relied on numerical techniques in both the frequency-domain and time-domain (Fig. 2), to determine the local instantaneous pressure distributions and mechanical impedances throughout an asymmetric branching airway tree, continuously during a breath. This combined approach was utilized in order to predict how nonlinear processes, such as R/D and overdistention, affect local and global mechanics of the injured lung within a single breath. The computation associated with the vast number of regional impedances, flows, pressures in the asymmetric airway tree used in this study is most easily accomplished in the frequency-domain [17, 25], given the computational efficiency of calculating and storing the mechanical impedances looking into each node of the tree [18]. Frequency-domain approaches also allow one easily to determine regional flow and pressure distributions throughout the tree [17, 25], which are required to determine whether any acinus in the model has been exposed to a critical opening or closing pressure. However, frequency-domain analyses have traditionally been constrained to describing the steady-state behavior of linear, time-invariant approximations of the respiratory system during sinusoidal excitation. While similar simulations can be performed in the time-domain, such models are generally limited to symmetric airway trees [30, 31] or simpler descriptions of parenchymal mechanics [32] due to tremendous computational burden associated with asymmetric trees and fractional viscoelasticity. By contrast, our model relies on the assumptions of piecewise linearity and time invariance over very small time scales, in order to quantify the effects of nonlinear R/D and overdistention on apparent global lung mechanics over a longer period of time.

Consistent with previous studies [33], our model predicts that the most injurious conditions for the lung occur during low PEEP and high V_T. Indeed Fig. 4 indicates that this condition is associated with the greatest number of acini in the transitional state, with nearly 80% of

acini experiencing intratidal R/D for 5 cm H_2O PEEP and 20 mL kg^{-1} V_T. The repetitive opening and closing of these transitional acini would thus be at the highest risk for atelectrauma. The histograms of acinar recruitment duty cycles (Fig. 5) provide additional information on the temporal occurrences of R/D phenomena for the population of transitional acini in the model. For example, we found that the number of transitional acini at a specified RDC increased with increasing V_T. Moreover, these transitional acini were shifted higher values of RDC with increasing V_T, indicating that these acini spent less time in a derecruited state during the course of a breath. Whether or not such behavior would impact the efficiency of gas exchange or the lung's propensity to ventilator-associated lung injury is unclear from these simulations.

Our simulations also support the notion of an 'optimal' distending pressure in the injured lung, for which the opposing factors of R/D and overdistention are appropriately balanced [34]. Variations in R_L, E_L, and $|Z_L|$ near minima reflect reduced mechanical stress. Below these minima, R_L, E_L, and $|Z_L|$ will increase with decreasing airway pressure, as more lung units are derecruited. Above these minima, the value of these parameters will increase as the lung parenchyma tends toward overdistention. While it may be difficult to determine a nonarbitrary and quantifiable definition for overdistention in our model, one may assume that significant pathologic overdistention would occur once 100% of the lung has been recruited, consistent with the large intratidal variations in R_L, E_L, and $|Z_L|$ (Fig. 6). Thus keeping airway pressure as close as possible to these corresponding minima, thus minimizing intratidal variations mechanical properties, may allow for the best compromise between the pathophysiologic processes of cyclic R/D and potential parenchymal overdistention. It should be noted, however, that ventilatory airway pressures near these minima do not necessarily imply maximal lung recruitment or minimal overdistention. In fact, our 'optimal' pressures of 15.6 cm H_2O (based on R_L) and 11.6 cm H_2O (based on E_L and $|Z_L|$) were associated with only about 41% and 45% lung recruitment, respectively. Moreover, the empiric relationships used to describe H_n and η_n as functions of transpulmonary pressure (Equations 1 and 2) were derived from the mechanics of healthy canine lungs [22]. Thus these optimal pressures may not show influence from possible surfactant dysfunction typical of lungs with ARDS. Nonetheless, these simulated optimal pressures are in fairly close quantitative agreement with studies of optimal pressures based on estimates of 'best' compliance, elastance, or reactance in other mammalian species with injured lungs [6, 7, 35–37].

Our simulations also illustrate that the concavity of the pressure-volume (P-V) curve of the injured lung does not reliably reflect processes of recruitment or overdistention, or predict where on the curve an optimal distending pressure might occur. Traditionally, the P-V curve of the injured lung can be described empirically with a sigmoidal function [28], with two points demarcated: the so-called 'upper inflection point' representing the point at which the majority of lung parenchyma experiences overdistention, and the 'lower inflection point' representing the process of maximum alveolar recruitment [38]. For our model, no discernable lower inflection point was observed in the simulated P-V loops, despite the fact that ongoing recruitment was occurring during inflation for pressures less than 28 cm H_2O (Fig. 8). Indeed, these dynamic P-V curves were relatively linear from 5 to 28 cm H_2O, regardless of PEEP or V_T. The upper inflection point could only be discerned for tracheal

pressures above 28 cm H_2O, after 100% of acini had been recruited. Above 28 cm H_2O the P-V curves demonstrated characteristic flattening, as the combined elastances of the individual acini increased with transpulmonary pressure according to (1).

We also investigated the sensitivity of two different nonlinear indices, κ_d and $\%E_3$, to detect acinar R/D and parenchymal overdistention. The κ_d index has been previously used to assess the strength of nonlinearities in the respiratory system, for lungs driven by both pure sinusoids [39] as well as certain types of broadband waveforms with sparse frequency content [26]. In our case, we used κ_d to assess the degree to which our tracheal pressure waveform deviated from a simple ideal sinusoid. As expected, κ_d demonstrated increases with both PEEP and V_T (Table I), as both intratidal R/D and overdistention are highly nonlinear phenomena. Thus, these processes result considerable harmonic distortion and spectral crosstalk in the resulting tracheal pressure waveform [26, 39–41]. However increases in κ_d alone did not distinguish between these two processes, or the relative extent to which either contributed to the nonlinear behavior. For example the greatest value of κ_d (35.4%) occurred at the highest level of both PEEP (15 cm H_2O) and V_T (20 mL kg^{-1}), a condition for which about 40% of the acini were transitional (at risk for atelectrauma) and 60% consistently recruited (at risk for volutrauma). However for the condition of 5 cm H_2O PEEP and 20 mL kg^{-1} V_T, the value of κ_d was 22.7%, which corresponded to about 25% consistently recruited acini and 75% transitional acini. Another limitation of the κ_d index is its lack of applicability to generalized broadband driving signals, such as volume-cycled or pressure-cycled ventilator waveforms.

Alternatively, the values of $\%E_3$ did appear to distinguish between intratidal R/D and overdistention (Table II). This index is based on the assumption that apparent lung recoil pressure may be adequately characterized by a third order polynomial relationship with volume (8). At the lowest PEEP level of 5 cm H_2O, intratidal R/D would be expected to dominate the nonlinear behavior of our model. In this case the value of $\%E_3$ was always negative, although its magnitude decreased with increasing V_T. By contrast at the highest PEEP of 15 cm H_2O, for which overdistention would be expected to dominate nonlinear behavior, $\%E_3$ was always positive and increased with increasing V_T. The smallest magnitude of $\%E_3$ (7.3%) occurred at the mid-level of PEEP (10 cm H_2O) and the lowest V_T (10 mL kg^{-1}), during which P_{tr} varied from 10 cm H_2O to just under 28 cm H_2O. This suggests that $\%E_3$ could have some clinical utility for the adjustment of PEEP or V_T in patients with ARDS, as it may be an additional indicator of the degree to which airway pressure is deviating from the so-called ‘optimal’ pressures of Fig. 7.

Several limitations of this model should be noted. First, we simulated the effects of PEEP and V_T on R/D and parenchymal overdistention over a very short time scale (i.e., a single breath). In reality, sudden changes in PEEP and V_T may manifest themselves over much longer time scales, and may require several breaths to achieve a steady-state [42]. Our model also assumes that recruitment or derecruitment of an acinus occurs instantaneously, when its distending pressure reaches a threshold critical opening or closing pressure, respectively. In reality, the recruitment or derecruitment processes may not be instantaneous, but rather may require seconds to minutes after an acinus has been exposed to such a critical pressure [24]. Nonetheless, there is strong experimental evidence to suggest that ongoing R/D occurs

within the time scale of a single breath [43]. Also for the sake of model simplicity, and to be consistent with the 'steady-state' level of recruitment measured by Kaczka et al. during small amplitude forced oscillations [13], we constrained the opening and closing pressures for each individual acinus to be equivalent. However, the actual opening and closing pressures for individual acini may be very different [24]. In addition, we restricted our volume forcings to pure sinusoidal waveforms, to simplify the computational burden associate with multiple conversions between the time-domain and frequency-domain during the course of a breath. In reality, ventilator waveforms are broadband periodic signals, with harmonics above the fundamental frequency of excitation [44]. While more realistic ventilator waveforms may be constructed from a superposition of multiple sinusoids [45], the computation of flow and pressure distributions throughout the airway tree would require considerably more processing time. Finally, our one dimensional airway network does not allow for anatomic specificity of lung injury [15]. Nonetheless the computational techniques detailed here can easily be extended to three dimensional airway trees, such that specific regions of lung injury can be assigned to distinct anatomic locations [46].

V. Conclusions

In summary, our model simulations demonstrate that stable lung recruitment depends on both static (PEEP) and dynamic (V_T) factors. While higher PEEP levels and high V_T yield more consistently recruited acini, increases in V_T are associated with increases in intratidal recruitment / derecruitment as well as the stresses associated with parenchymal overdistention. Titration of airway pressures based on variations in intratidal mechanics may therefore minimize the processes associated with Ventilator-Associated Lung Injury.

Acknowledgments

This work was supported in part by National Institutes of Health Grants HL112547 (RA), and HL108724 (DWK).

Portions of these simulations were performed while the authors were affiliated with Beth Israel Deaconess Medical Center and Harvard Medical School, Boston, MA.

Glossary of Nomenclature

ARDS	Acute Respiratory Distress Syndrome
E_1,E_2, E_3	polynomial coefficients of lung elastance
E_L	total lung elastance
f	breathing frequency in Hz
H_n	tissue elastance of acinus n
j	unit imaginary number (i.e., $\sqrt{-1}$)
k	index for nodes (airway segments) in binary tree
K	total number of airway segments in model (300,153)
κ_d	harmonic distortion index

n	acinar index
N	total number of acini in the model (150,077)
$P_{crit,n}$	critical opening / closing pressure of acinus n
P_k	local pressure at airway node k
$\|P_k\|$	magnitude of local pressure at airway node k
PEEP	positive end-expiratory pressure
$P_{tp,n}$	transpulmonary pressure of acinus n
P_{tr}	tracheal pressure
$\mathcal{P}_{ni}$	spectral power of P_{tr} for harmonics above the ventilation frequency
$\mathcal{P}_{tot}$	total spectral power of P_{tr}
R	linear coefficient of lung resistance
R/D	recruitment / derecruitment
$\mathbf{RDC}_n$	recruitment duty cycle of acinus n
R_L	total lung resistance
t	time index in seconds
$T_{rec,n}$	time that acinus n remains in a recruited state
T_{tot}	total time period of a breath
V_T	tidal volume
V_{tr}	volume delivered at the trachea
$\dot{V}_{tr}$	tracheal flow
$\|\dot{V}_{tr}\|$	magnitude of tracheal flow
X_L	total lung reactance
Z_L	total lung impedance
$\|Z_L\|$	magnitude of total lung impedance
η_n	tissue hysteresivity of acinus n
π	number of radians in a semi-circle
ϕ_k	phase of local pressure at airway node k

References

1. The ARDS Network. Ventilation with lower tidal volumes as compared with traditional tidal volumes for acute lung injury and the acute respiratory distress syndrome. N Engl J Med. 2000; 342:1301–1308. [PubMed: 10793162]
2. Brower RG, et al. Higher versus lower positive end-expiratory pressures in patients with the acute respiratory distress syndrome. N Engl J Med. 2004; 351:327–336. [PubMed: 15269312]
3. Ranieri VM, et al. Pressure-time curve predicts minimally injurious ventilatory strategy in an isolated rat lung model. Anesthesiology. 2000; 93:1320–1328. [PubMed: 11046222]
4. Carvalho AR, et al. Ability of dynamic airway pressure curve profile and elastance for positive end-expiratory pressure titration. Intensive Care Med. Dec.2008 34:2291–9. [PubMed: 18825365]
5. Zannin E, et al. Optimizing positive end-expiratory pressure by oscillatory mechanics minimizes tidal recruitment and distension: an experimental study in a lavage model of lung injury. Crit Care. Nov.2012 16:R217. [PubMed: 23134702]
6. Zannin E, et al. Optimal mean airway pressure during high-frequency oscillatory ventilation determined by measurement of respiratory system reactance. Pediatr Res. Apr.2014 75:493–9. [PubMed: 24375086]
7. Carvalho AR, et al. Positive end-expiratory pressure at minimal respiratory elastance represents the best compromise between mechanical stress and lung aeration in oleic acid induced lung injury. Crit Care. 2007; 11:R86. [PubMed: 17688701]
8. Carvalho AR, et al. Volume-independent elastance: a useful parameter for open-lung positive end-expiratory pressure adjustment. Anesth Analg. 2013; 116:627–633. [PubMed: 22467900]
9. Carvalho AR, et al. Detection of tidal recruitment/overdistension in lung-healthy mechanically ventilated patients under general anesthesia. Anesth Analg. Mar.2013 116:677–84. [PubMed: 22543064]
10. Talmor D, et al. Mechanical ventilation guided by esophageal pressure in acute lung injury. N Engl J Med. 2008; 359:2095–2104. [PubMed: 19001507]
11. Loring SH, et al. Esophageal pressures in acute lung injury: do they represent artifact or useful information about transpulmonary pressure, chest wall mechanics, and lung stress? J Appl Physiol. 2010; 108:512–522.
12. Kaczka DW, et al. Analysis of regional mechanics in canine lung injury using forced oscillations and 3D image registration. Ann Biomed Eng. 2011; 39:1112–1124. [PubMed: 21132371]
13. Kaczka DW, et al. Quantifying mechanical heterogeneity in canine acute lung injury: Impact of mean airway pressure. Anesthesiology. 2005; 103:306–317. [PubMed: 16052113]
14. Amini, R., Kaczka, DW. Effects of intratidal overdistention and derecruitment on global lung mechanics: A simulation study. The Biomedical Engineering Society Annual Meeting; Austin, TX. 2010. p. 69
15. Horsfield K, et al. An asymmetrical model of the airways of the dog lung. J Appl Physiol. 1982; 52:21–26. [PubMed: 7061267]
16. Thorpe CW, Bates JHT. Effect of stochastic heterogeneity on lung impedance during acute bronchoconstriction: a model analysis. J Appl Physiol. 1997; 82:1616–1625. [PubMed: 9134912]
17. Amini R, Kaczka DW. Impact of ventilation frequency and parenchymal stiffness on flow and pressure distribution in a canine lung model. Ann Biomed Eng. 2013; 41:2699–2711. [PubMed: 23872936]
18. Kaczka DW, et al. Reliability of estimating stochastic lung tissue heterogeneity from pulmonary impedance spectra: a forward-inverse modeling study. Ann Biomed Eng. 2007; 35:1722–1738. [PubMed: 17558554]
19. Habib RH, et al. Serial distribution of airway mechanical properties in dogs: effects of histamine. J Appl Physiol. 1994; 77:554–566. [PubMed: 8002500]
20. Hantos Z, et al. Input impedance and peripheral inhomogeneity of dog lungs. J Appl Physiol. 1992; 72:168–178. [PubMed: 1537711]
21. Fredberg JJ, Stamenovic D. On the imperfect elasticity of lung tissue. J Appl Physiol. 1989; 67:2408–2419. [PubMed: 2606848]

22. Kaczka DW, Smallwood JL. Constant-phase descriptions of canine lung, chest wall, and total respiratory viscoelasticity: effects of distending pressure. Respir Physiol Neurobiol. 2012; 183:75–84. [PubMed: 22691447]
23. Barnas GM, et al. Lung tissue and airway impedance during pulmonary edema in the normal range of breathing. J Appl Physiol. 1995; 78:1889–1897. [PubMed: 7649927]
24. Bates JHT, Irvin CG. Time dependence of recruitment and derecruitment in the lung: a theoretical model. J Appl Physiol. 2002; 93:705–713. [PubMed: 12133882]
25. Colletti AA, et al. Simulating ventilation distribution in heterogeneous lung injury using a binary tree data structure. Comput Biol Med. 2011; 41:936–945. [PubMed: 21872852]
26. Zhang Q, et al. Harmonic distortion from nonlinear systems with broadband inputs: applications to lung mechanics. Ann Biomed Eng. 1995; 23:672–681. [PubMed: 7503467]
27. Kaczka DW, et al. Assessment of time-domain analyses for estimation of low-frequency respiratory mechanical properties and impedance spectra. Ann Biomed Eng. 1995; 23:135–151. [PubMed: 7605051]
28. Venegas JG, et al. A comprehensive equation for pulmonary pressure-volume curve. J Appl Physiol. 1998; 84:389–395. [PubMed: 9451661]
29. Kano S, et al. Influence of nonlinearities on estimates of respiratory mechanics using multilinear regression analysis. J Appl Physiol. 1994; 77:1185–1197. [PubMed: 7836121]
30. Venegas JG, et al. Self-organized patchiness in asthma as a prelude to catastrophic shifts. Nature. 2005; 434:777–782. [PubMed: 15772676]
31. Pedley TJ, et al. The prediction of pressure drop and variation of resistance within the human bronchial airways. Respir Physiol. 1970; 9:387–405. [PubMed: 5425201]
32. Nucci G, et al. A morphometric model of lung mechanics for time-domain analysis of alveolar pressures during mechanical ventilation. Ann Biomed Eng. 2002; 30:537–545. [PubMed: 12086004]
33. Seah AS, et al. Quantifying the roles of tidal volume and PEEP in the pathogenesis of ventilator-induced lung injury. Ann Biomed Eng. 2011; 39:1505–1516. [PubMed: 21203845]
34. Dellacà RL, et al. Optimisation of positive end-expiratory pressure by forced oscillation technique in a lavage model of acute lung injury. Intensive Care Med. 2011; 37:1021–1030. [PubMed: 21455750]
35. Kostic P, et al. Positive end-expiratory pressure optimization with forced oscillation technique reduces ventilator induced lung injury: a controlled experimental study in pigs with saline lavage lung injury. Crit Care. 2011; 15:R126. [PubMed: 21575220]
36. Bellardine-Black CL, et al. Relationship between dynamic respiratory mechanics and disease heterogeneity in sheep lavage injury. Crit Care Med. 2007; 35:870–878. [PubMed: 17255854]
37. Suarez-Sipmann F, et al. Use of dynamic compliance for open lung positive end-expiratory pressure titration in an experimental study. Crit Care Med. Jan.2007 35:214–21. [PubMed: 17110872]
38. Hickling KG. The pressure-volume curve is greatly modified by recruitment. A mathematical model of ARDS lungs. Am J Respir Crit Care Med. 1998; 158:194–202. [PubMed: 9655729]
39. Suki B, et al. Nonlinearity and harmonic distortion of dog lungs measured by low-frequency forced oscillations. J Appl Physiol. 1991; 71:69–75. [PubMed: 1917766]
40. Suki B. Nonlinear phenomena in respiratory mechanical measurements. J Appl Physiol. 1993; 74:2574–2584. [PubMed: 8335594]
41. Suki B, Lutchen KR. Pseudorandom signals to estimate apparent transfer and coherence functions of nonlinear systems: applications to respiratory mechanics. IEEE Trans Biomed Eng. 1992; 39:1142–1151. [PubMed: 1487277]
42. Allen G, et al. Transient mechanical benefits of a deep inflation in the injured mouse lung. J Appl Physiol. 2002; 93:1709–1715. [PubMed: 12381758]
43. Crotti S, et al. Recruitment and derecruitment during acute respiratory failure: a clinical study. Am J Respir Crit Care Med. Jul.2001 164:131–40. [PubMed: 11435251]
44. Lutchen KR, et al. Low-frequency respiratory mechanics using ventilator-driven forced oscillations. J Appl Physiol. 1993; 75:2549–2560. [PubMed: 8125874]

45. Barnas GM, et al. Influence of waveform and analysis technique on lung and chest wall properties. Respir Physiol. 1994; 96:331–344. [PubMed: 8059094]

46. Tawhai MH, et al. The lung physiome: merging imaging-based measures with predictive computational models. Wiley Interdiscip Rev Syst Biol Med. 2009; 1:61–72. [PubMed: 20835982]

Biographies

Reza Amini received his Ph.D. in mechanical engineering from Northeastern University in Boston, MA in 2007. He was a postdoctoral research fellow in the Department of Anesthesiology & Critical Care Medicine at Johns Hopkins University in Baltimore, MD and a research fellow at Beth Israel Deaconess Medical Center and Harvard Medical School in Boston, MA. He is currently a Senior Analyst at Cimetrics, Inc. in Boston, MA.

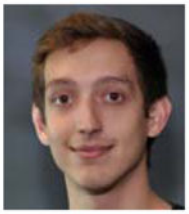

Jacob Herrmann received the B.S. (*magna cum laude*) and M.S. degrees in biomedical engineering from Boston University in Boston, MA in 2012 and 2015, respectively. He is currently a candidate for the Ph.D. degree in biomedical engineering at the University of Iowa in Iowa City, IA. His research interests include computational modeling of respiratory structure and function based imaging and physiologic measurements.

David W. Kaczka is an Associate Professor of Anesthesia, Biomedical Engineering, and Radiology at the University of Iowa. He received the B.S. (*summa cum laude*), M.S., and Ph.D. degrees in biomedical engineering from Boston University College of Engineering in 1990, 1993, and 2000 respectively, as well as the M.D. degree from Boston University School of Medicine in 2000. He completed his residency in anesthesiology at Johns Hopkins University in 2004. Dr. Kaczka has held previous faculty appointments Johns Hopkins University and Harvard Medical School. His current research interests include

computational modeling of respiratory mechanics and gas exchange, design and function of mechanical ventilators, patient monitoring, and image processing.

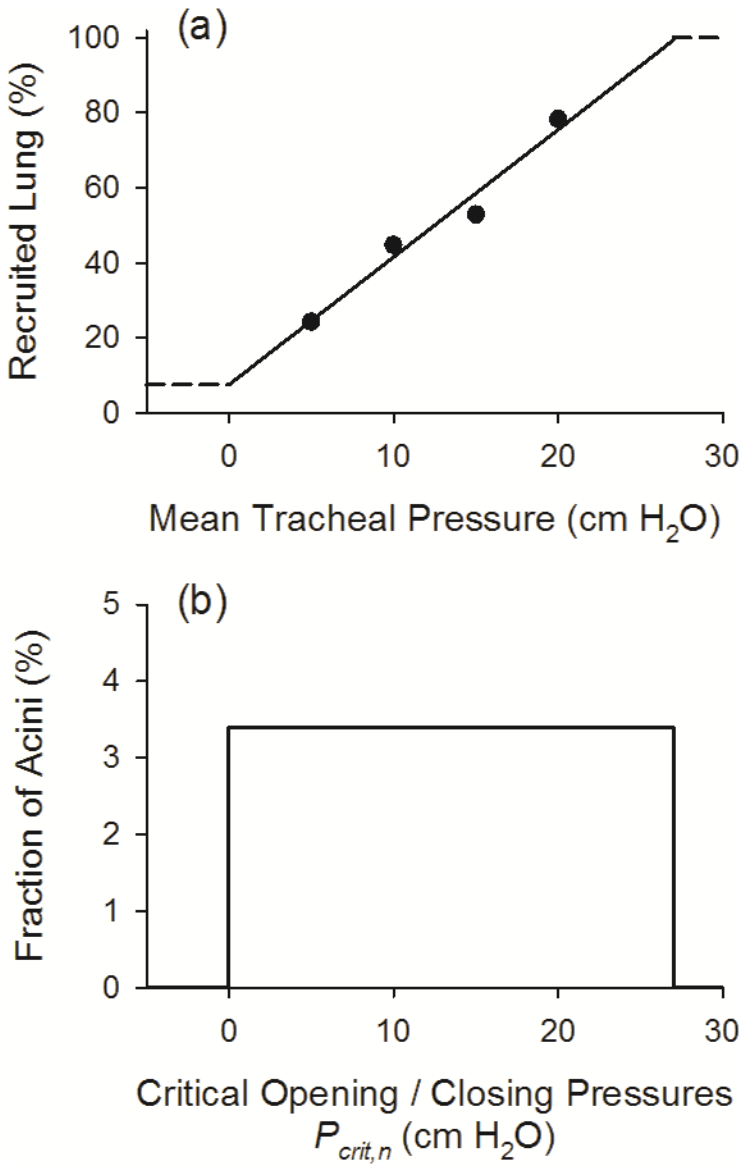

Fig. 1.

(a) Percentage of recruited lung vs. mean tracheal pressure. Symbols are computed from the experimental data of Kaczka et al. [13], as the ratio healthy to injured dynamic elastance multiplied by 100%. Solid line is the linear regression for the four data points, with horizontal dashed lines denoting the imposed upper and lower limits of recruitment. Thus the model assumes that 7.6% of the lung is recruited at a mean tracheal pressure of 0 cm H_2O, while 100% of the lung is recruited at about 28 cm H_2O. (b) Distribution of acinar critical opening / closing pressures ($P_{crit,n}$), expressed as the fraction of total acini in the model. This distribution is computed as the slope (i.e., derivative) of the function in (a).

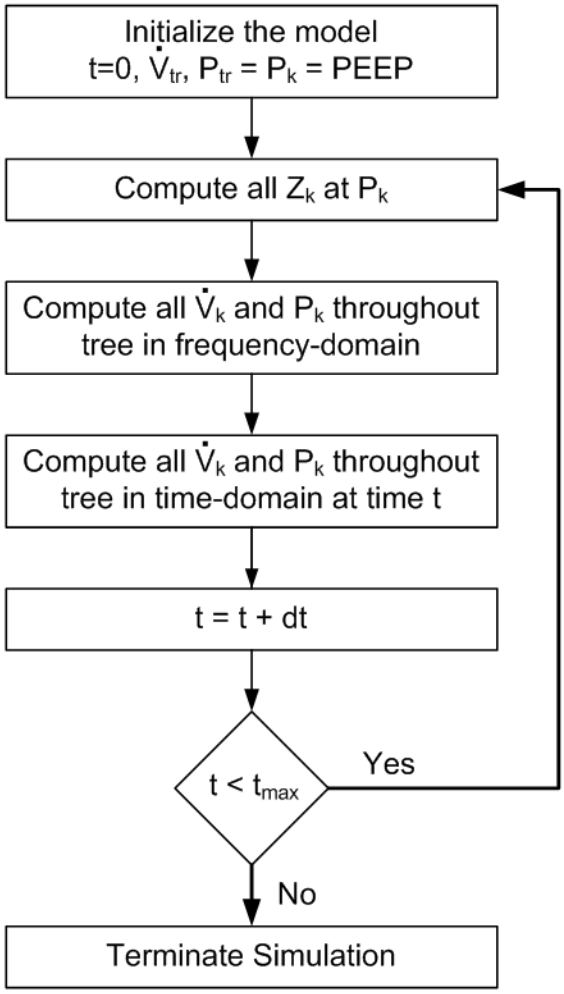

Fig. 2.

Algorithm used to simulate time-domain variations in flow and pressure based on nonlinear variations in impedance. At time $t = 0$, the model is initiated by setting a PEEP and sinusoidal tracheal flow magnitude $|\dot{V}_{tr}|$. The local impedances throughout the tree (Z_k) are then computed at this PEEP. Regional pressure magnitudes (P_k) and phases (ϕ_k) throughout the tree are determined in frequency-domain, and then converted to time-domain values according to (4). The time index is then incremented as $t = t + dt$.

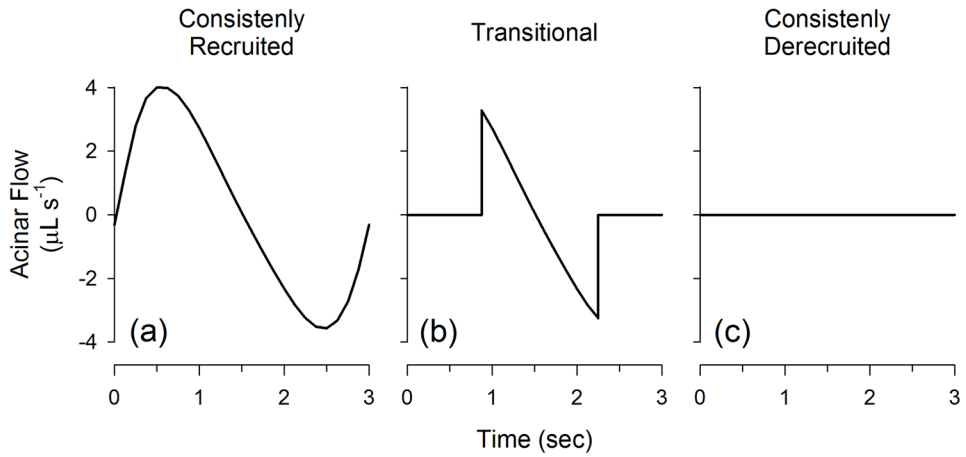

Fig. 3.

Acinar flow patterns in the model are divided into three distinct subgroups: (a) consistently recruited; (b) transitional; and (c) consistently derecruited.

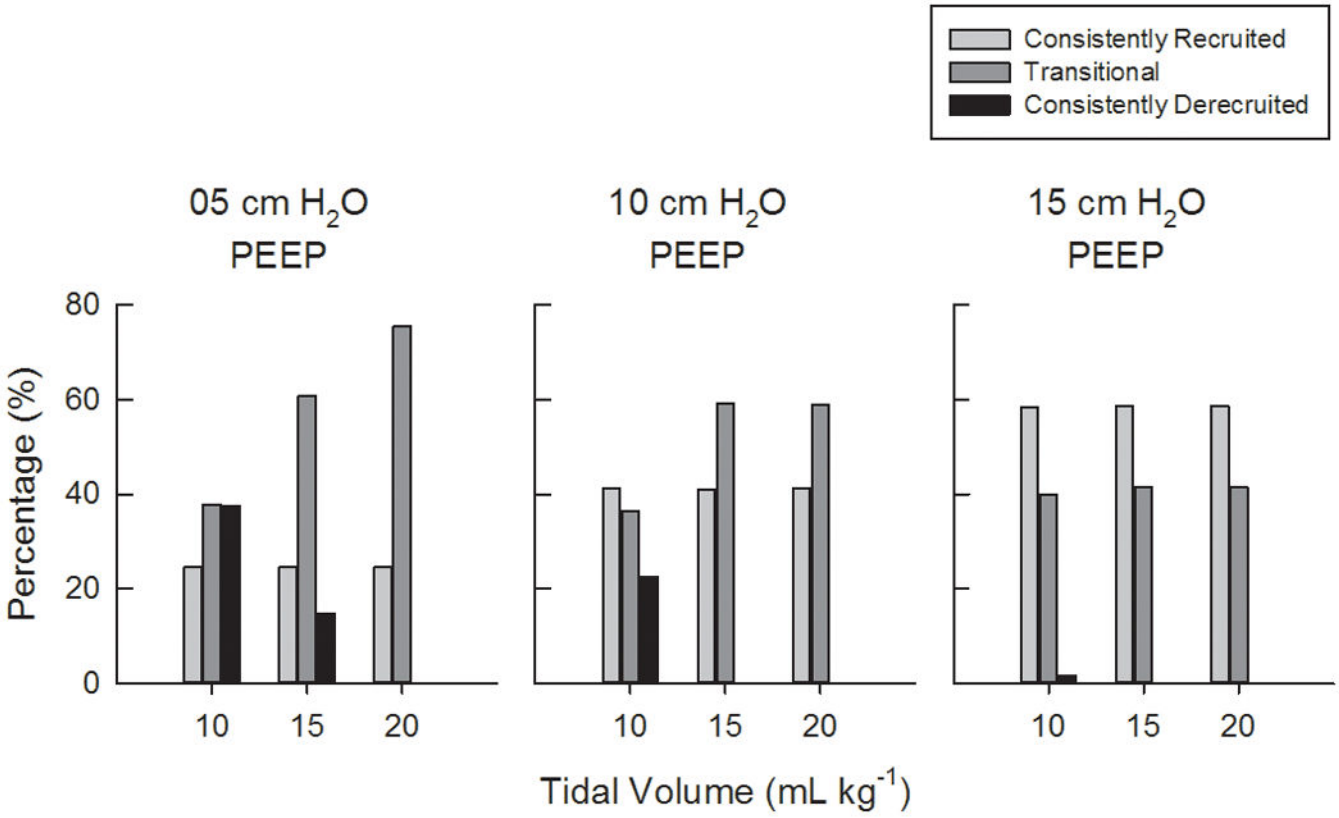

Fig. 4.

Percentages of consistently recruited, transitional, and consistently derecruited acini in the model for 5, 10, and 15 cm H_2O PEEP and 10, 15, and 20 mL kg^{-1} V_T.

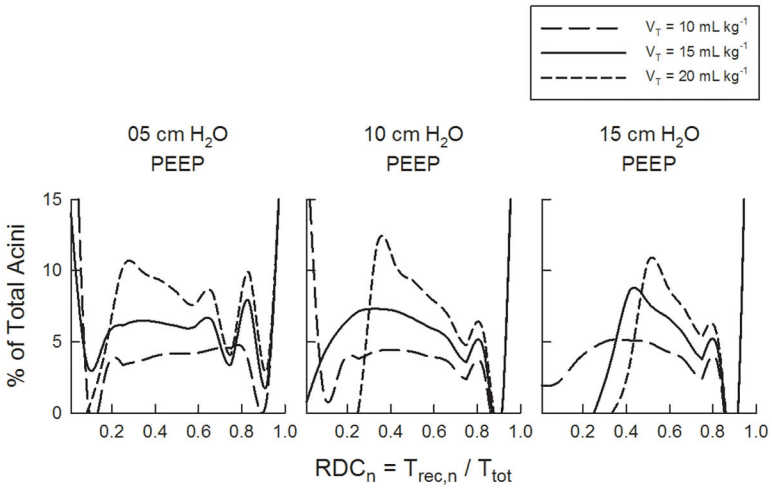

Fig. 5.

Histograms of the acinar recruitment duty cycle (RDC$_n$), defined as the fraction of time that acinus stays opened throughout a breath. Histograms are shown for PEEPs of (a) 5, (b) 10, and (c) 15 cm H_2O, and tidal volumes of 10, 15, and 20 mL kg^{-1}.

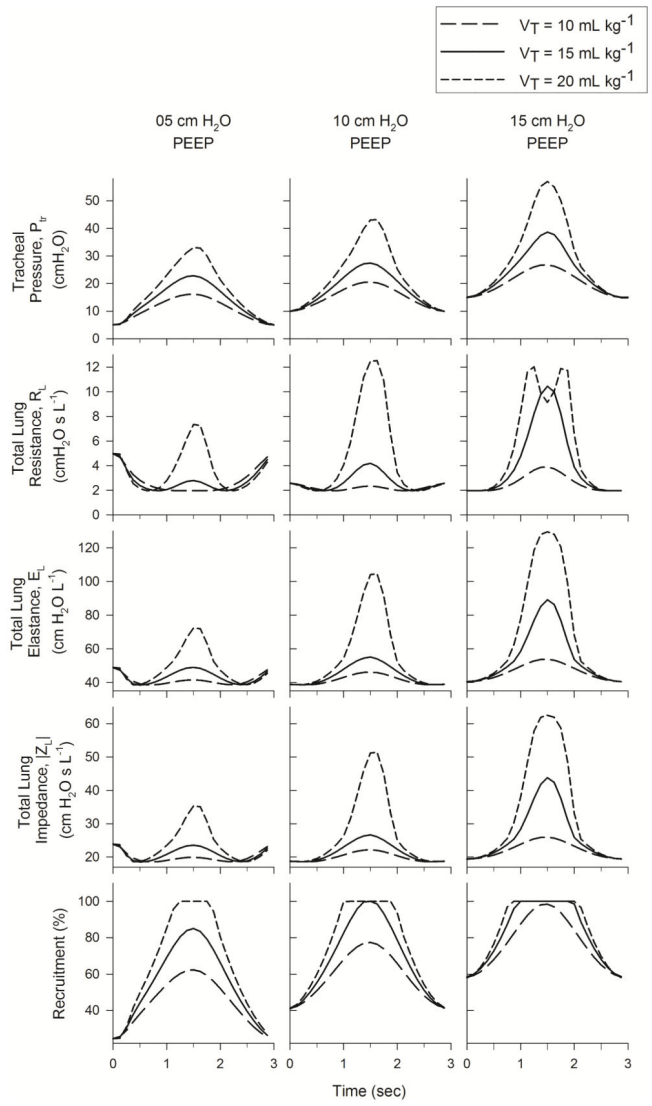

Fig. 6.

Tracheal pressure variations and within breath variations of lung resistance, elastance, impedance, and acinar recruitment for 5, 10, and 15 cm H_2O PEEP and 10, 15, and 20 mL kg^{-1} V_T.

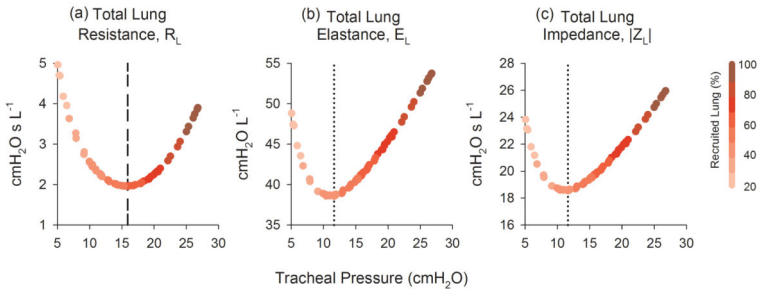

Fig. 7.

(a) Total lung resistance (R_L), (b) elastances (E_L), and (c) impedance magnitude ($|Z_L|$) as functions of tracheal pressure. Trajectories are color coded (shaded) to denote the percentage of recruited lung as a function of tracheal pressure. Vertical dashed /dotted lines denote 'optimal' tracheal pressures, according to the pressure for which R_L, E_L, or $|Z_L|$ is minimized.

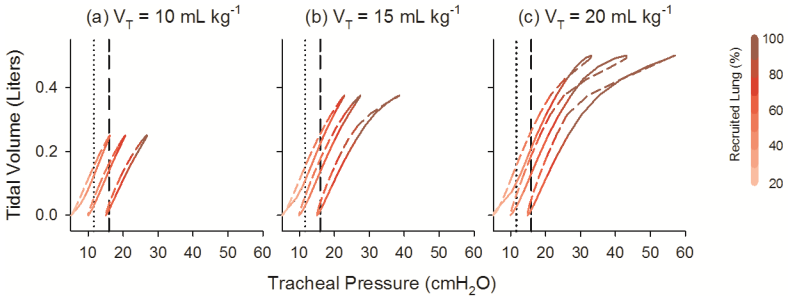

Fig. 8.

Simulated dynamic pressure-volume loops for single breaths at (a) 10, (b) 15, and (c) 20 mL kg^{-1} and 5, 10, and 15 cm H_2O PEEP (left to right within each panel). Loops are color coded (shaded) to denote the percentage of recruited lung during the course of a breath. Solid lines denote inspiration, while dashed lines denote expiration. Vertical lines denote 'optimal' tracheal pressure, as defined according to the minimum E_L or $|Z_L|$ (11.6 cm H_2O, dotted line) or R_L minimum (15.9 cm H_2O, dashed line) criteria (Fig. 7).

Table I

percent harmonic distortion (κ_d) for tracheal pressure waveforms of the model at three PEEP levels (5, 10, and 15 cm H_2O) and three tidal volumes (10, 15, and 20 mL kg^{-1}), as computed using the method of Zhang et al. [26].

Tidal Volumes	05 cm H_2O PEEP	10 cm H_2O PEEP	15 cm H_2O PEEP
10 mL kg^{-1}	7.53	8.98	11.3
15 mL kg^{-1}	11.1	13.8	26.5
20 mL kg^{-1}	22.7	33.4	35.4

Table II

Nonlinear volume-dependent elastance index (%E_3) at three PEEP levels (5, 10, and 15 cm H_2O) and three tidal volumes (10, 15, and 20 mL kg^{-1})

Tidal Volumes	05 cm H_2O PEEP	10 cm H_2O PEEP	15 cm H_2O PEEP
10 mL kg^{-1}	−52.2%	7.3%	20.9%
15 mL kg^{-1}	−40.9%	15.5%	21.6%
20 mL kg^{-1}	−26.0%	14.9%	36.8%